Thee-Dimensional Control of Helical Magnetic Microrobots using Two Synchronized Rotating Dipole Fields

Bachelor Thesis

German University in Cairo

Faculty of Material Science and Engineering

Mechatronics Engineering

Author:

Abdelrahman Hosney

Supervisors:

Dr. Islam Khalil

Dr. Anke Klinge

ACKNOWLEDGMENTS

It is with immense gratitude that I acknowledge the support and help of my supervisor Professor Islam Khalil who believed in me and was continuously supporting me in every problem that occurred during this research. Our cooperation was truly an inspiring experience. Very special thanks to Proffesor Anke Klingner for her eagerness and great assistance; her comments were of critical importance. Special thanks goes to my friends, Mahmoud Alshafeei, Abdelrahman Alfar, Youssef Michel, Hussein El-Safy, Abdelrahman Osman, Micheal Maher, Ahmed Abdelsamad, and Farah Noaman for their advice, patience and hard work that made this thesis possible. I would like to dedicate this work to my beloved parents, Mohamed Hosney, Sohaila Maged and my sister, Khadiga Hosney. Without your love and support I could not have made it until the end. Finally I'd like to thank Mariam Soliman who always believed in me, was always there and always will be. I owe you all everything.

To the memory of my father, Mohamed H. Youssef.

TABLE OF CONTENTS

Page

LIST OF FIGURES

Figure Page

Figure Page

SYMBOLS

m	Mass
v	Velocity
$F()$	Magnetic force
$T()$	Magnetic torque
$B()$	Magnetic field
$M()$	Magnetization of the helical microrobot
∇	Gradient operator
$\vec{u_t}$	Axis of rotating magnetic field
t	Time
ϕ	Inclination angle of helical microrobot
θ	Direction angle of helical microrobot
R	Radius of the permanent magnet
L	Thickness of the permanent magnet
μ_0	The vacuum permeability constant

ABSTRACT

Our analytical model using the finite elements method prove that our system the two synchronized dipole fields is capable of controlling the helical microrobot with average diameter of 500 μm in two-dimensional (2D) and three-dimensional (3D) spaces . the helical microrobot is capable of being controlled in these situations as opposed to a single rotating dipole field, when the x-axis gradient forces are mitigated from the use of two synchronized rotating dipole fields, and what remains of the gradient forces is compensated using propulsion force, the helical microrobot also compensated for gravity using the y-axis component of the propulsion force, and we observe that the helical microrobot compensates for gravity at $\phi = 63°$where it swims at an average speed of 0.25 body lengths per second. The helical microrobot when controlled in the two synchronized rotating dipole fields system, an innovative steering strategy is used, where the helical robot in the XZ plane is steered in the opposite direction of the rotation of the end effector, while the rotation in the YZ plane and the XY plane is the same as the rotation of the end effectors.

1. INTRODUCTION

Microrobots show great potential for future medical application, such as targeted drug delivery and minimally invasive surgery, which could provide a localized cure for cancer, or removal of arterial plaque. However, creating a robot in such a small scale requires the robot's design to be as minimal as possible [1] to be scalable to a smaller scale and many microrobots have been designed to tackle this problem, such as magnetosperms [2], microparticles [3], magnetotactic bacteria [4] and helical robots [5] [6] [7], each presenting its own advantages.

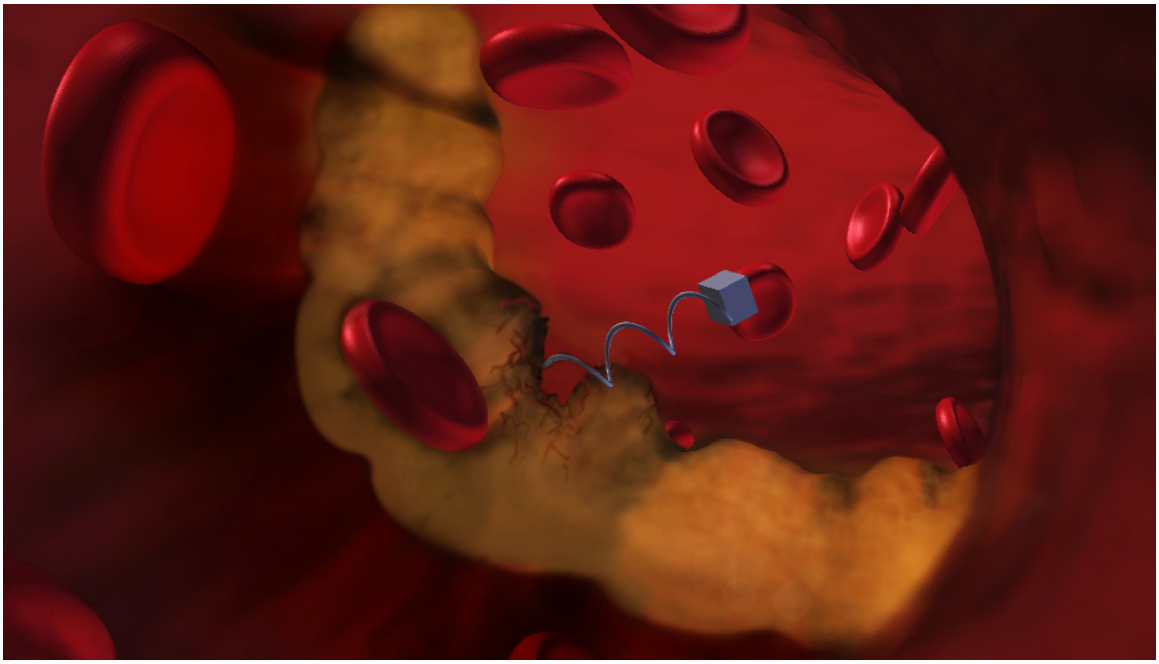

Fig. 1.1. Illustration of a helical microrobot drilling through arterial plaque

Microrobots [4] are faced with challenges that need to be met, before being applied to vivo applications. One of these challenges is that the systems that control these

microrobots tend to be built in a closed configuration, and aren't scalable to be big enough to control microrobots in a human body.

The helical microrobot is inspired from the E-coli bactera which uses an interesting locomotion strategy of rotating it's flagella, which proved to be a good propulsion strategy for locomotion in low reynolds number liquid, the helical microrobot's locomotion strategy allows it to be controlled under low magnetic fields of 10-20mT, this magnetic field needs to be rotating so that the helical microrobot is to synchronously rotate with the field as long as the magnetic torque is larger than the the drag torque, through clever manipulation of this rotating magnetic field the helical microrobot is controled using the magnetic torque which is proportional to the magnetic field, not the gradient of a field, making us more capable of building a scalable system.

Different systems were devised to control the helical robot, such as the helmholtz coil [8], the octomag [9] and a single rotating dipole field [10] [11]. However, the single rotating dipole field system has a problem from the magnetic force where the robot is only controlable if this force is canceled out from the gravitational force, so a system was built to allow for zero gradient point, and the reduction of the gradient forces throughout the workspace.

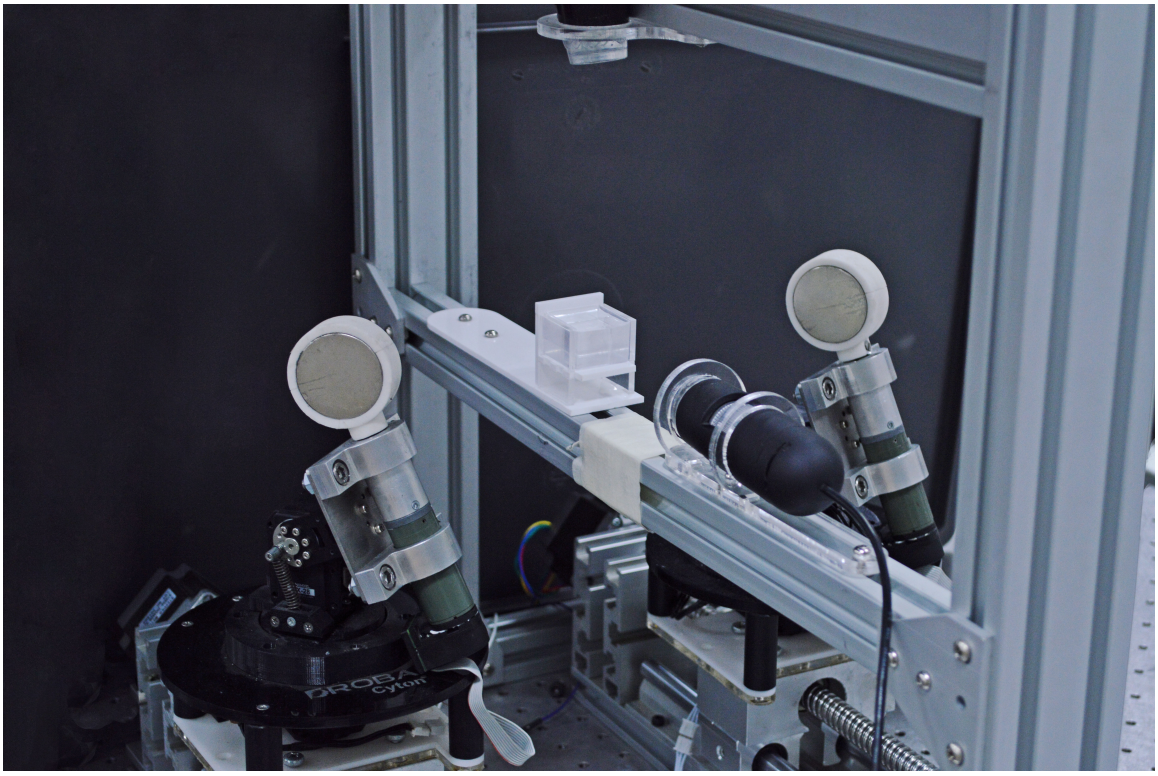

Fig. 1.2. Magnetic based robotic system to control helical microrobot's propulsion and steering in three-dimensional space

We have build an open configuration however building a novel system capable of controlling the helical robot in three-dimensional space which would require some challenges to be met, we needed to develop a steering strategy, that is robust enough to work throughout the workspace, the gradient of the magnetic field needs to be mitigated and the force from the magnetic field gradient to be compensated, the gravity forces need to be compensated as well, if the microrobot is to be controlled in three dimensional space, meeting these challenges is what we will be concerned with through this dissertation.

2. MAGNETIC FIELD ANALYSIS

The system needed to be studied how the rotation and position of the end effectors in the robotics system affect the direction and inclination steering of a helical microrobot and its propulsion. We can know that through studying how the magnetic field and its gradient are changed in the workspace when the end effector is moved.

The magnetic field and its gradient were analyzed in the area surrounding point P(Mid point between end effectors). They were then plotted and it was confirmed that a resultant magnetic force is induced on the helical microswimmer and this magnetic force. However, this magnetic force will hinder the control of the helical robot. The analytical results confirm the results from the previous paper; adding a synchronized dipole field does cancel out the gradient at point P. Thus, it mitigates magnetic forces at that point, giving us an area surrouding this point, where the force is negligible.

The linear propulsion characteristics of helical swimmers using permanent magnets were studied in our previous work; however, both the direction and inclination steering remained unstudied. Steering of helical microswimmers has shown in previous papers to be a challenge, due to their high surface to volume ratio. Nevertheless, steering of the helical swimmer using permanent magnets remains unstudied.

The steering of a helical robot, using synchronized dipole fields, would be achieved by changing the orientation of the end effector, but since the end effector will be moving in 3D space when it is being oriented, the gradient in the area being studied will change, exerting forces on the helical microwswimmer, so this report will be concerned if these magnetic forces can be used to improve the 3D steering strategy, or it will hinder the control.

2.1 Magnetic force

Magnetic force applied on the helical microrobot from the magnetic field caused by the rotating dipoles can be expressed as

$$\vec{F_t}(\vec{P}) = (\vec{M_t}.\nabla)\vec{B_t}(\vec{P})$$

The magnetic force $\vec{F_t}(\vec{P})$ is applied on the helical microrobot at point P, where the magnetization of the helical microrobot is noted as $\vec{M_t}$, and the magnetic field is noted as B_t and ∇ is the gradient operator.

When using two dipole fields we get at the mid point between both dipoles point P, we get the following equality.

$$\frac{\partial \vec{B_t}(\vec{P})}{\partial x} = \frac{\partial \vec{B_t}(\vec{P})}{\partial y} = \frac{\partial \vec{B_t}(\vec{P})}{\partial z} = 0$$

We get at P a pure magnetic torque on the magnetic dipole of the helical robot while the magnetic force is mitigated.

2.2 Magnetic torque

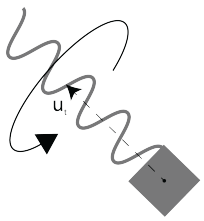

The helical microrobot rotates synchronously in the opposite direction of the rotating of the dipole field $\vec{u_t}$. It propels itself along the axis $\vec{u_t}$. Both $\vec{M_t}$ and $\vec{B_t}$ are perpendicular to the axis $\vec{u_t}$ at all times. The magnetic torque applied on the helical microrobot $\vec{T_t}$ can be expressed as:

$$\vec{T_t}(\vec{P}) = \vec{M_t} \times \vec{B_t}(\vec{P})$$

The torque $\vec{T_t}$ is applied in the direction of $\vec{u_t}$, which keeps the helical microrobot rotating synchronously around $\vec{u_t}$, and propelling itself forward or backward depending on the helical structure and the direction of rotation. At time t_+, the axis of the rotating magnetic field is changed to $\vec{u_{t+}}$. The magnetic field $\vec{B_{t+}}$ becomes perpendicular to $\vec{u_{t+}}$. However, the magnetization of the helical microrobot $\vec{M_{t+}}$ is still perpendicular to the initial axis $\vec{u_{t+}}$. The magnetic torque $\vec{T_{t+}}$ exerted on the helical microrobot, after the axis change of the rotating magnetic field, can be now expressed as:

$$\vec{T_{t+}}(P) = \vec{M_{t+}} \times \vec{B_{t+}}(P)$$

where the magnetic field can be decomposed in the directions perpendicular and parallel to the direction of $\vec{u_t}$. Then, the magnetic field $\vec{B_{t+}}$ can be expressed as:

$$\vec{B} = \vec{B_{\perp u_t}} + \vec{B_{\parallel u_t}}$$

2.3 Steering using magnetic torque

The magnetic torque exerted on the helical microrobot, after the axis of the rotating magnetic field changes, can be expressed as

$$\vec{T_{t+}}(P) = \vec{M_{t+}} \times \vec{B_{\perp u_t}}(P) + \vec{M_{t+}} \times \vec{B_{\parallel u_t}}(P)$$

The magnetization M_t+ is perpendicular to the $\vec{u_{t+}}$ direction, this magnetic torque can be decomposed in the directions perpendicular and parallel to $\vec{u_{t+}}$ as well. Torque $\vec{T_{\parallel u_t}}$ is the magnetic torque in the direction of $\vec{u_t}$, which makes the helical microrobot rotate around its actual axis $\vec{u_t}$. The magnetic torque $\vec{T_{\parallel u_t}}$ is the magnetic torque perpendicular to $\vec{u_t}$, which makes the helical microrobot rotate around the direction of $\vec{u_t} \times \vec{M_t}$. That means the direction of the axis of the helical microrobot changes.

2.4 Steering of the helical robot in the ZY plane using two synchronized dipole fields

The act of changing the axis direction from $\vec{u_t}$, to $\vec{u_{t+}}$ of the helical microrobot is called steering, in the next figures it can be observed how the helical microrobot is steered with the rotation of the end effector.

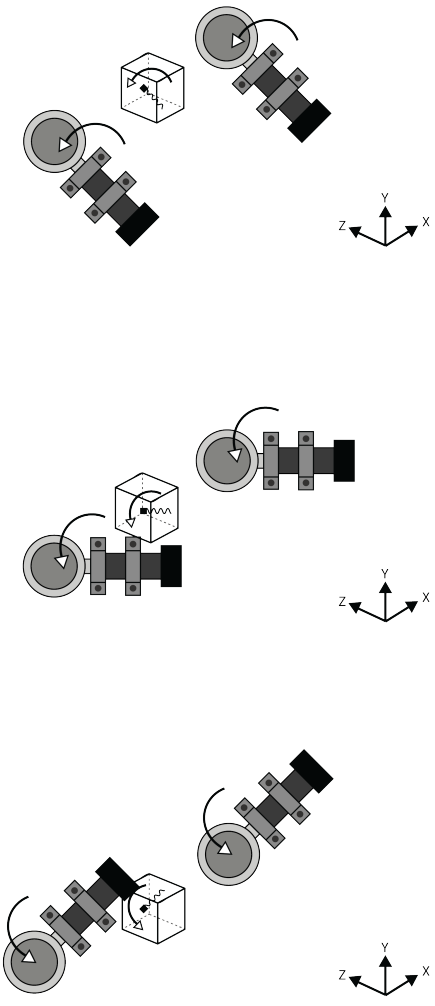

Fig. 2.1. Steering of a helical microrobot in the ZY plane moving with a forward propulsion

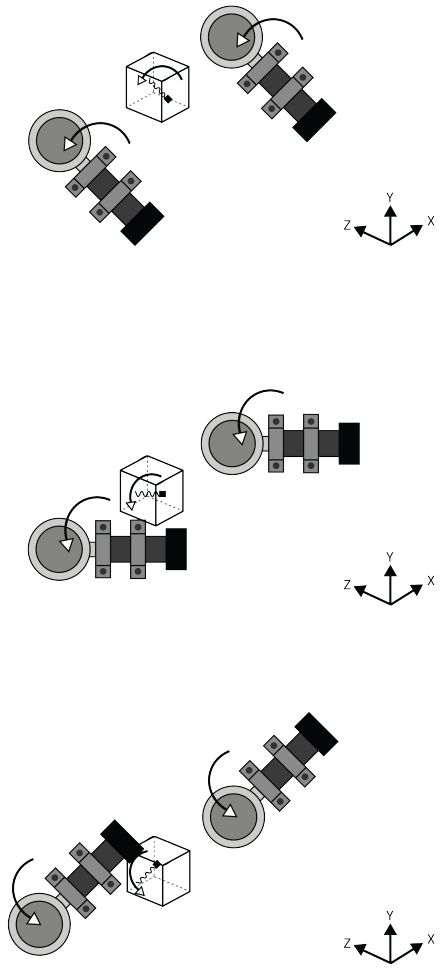

Fig. 2.2. Steering of a helical microrobot in the ZY plane moving with a backwards propulsion

2.4.1 Gravity compensation

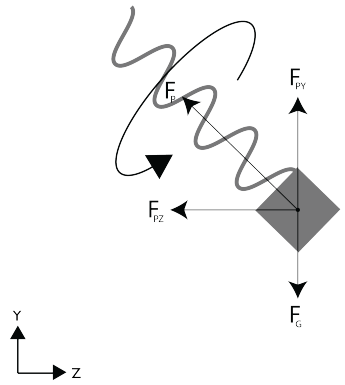

Fig. 2.3. The gravitation force can be mitigated using the Y-axis component of the propulsion force

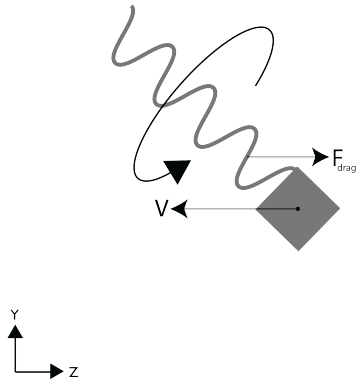

Fig. 2.4. the robot then propels itself in the negative Z-axis direction

2.5 Steering of the helical robot in the XZ plane using two synchronized dipole fields

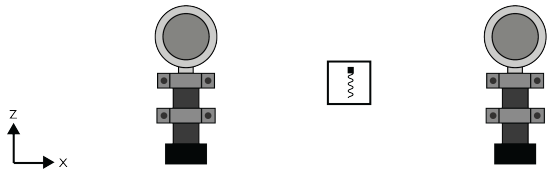

Fig. 2.5. Initial position of the system

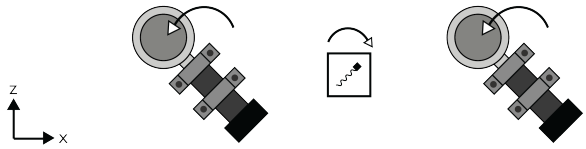

Fig. 2.6. Counter clock-wise movement of end effectors to 45°, causes the helical microrobot to be steered in the opposite direction

Fig. 2.7. Counter clock-wise movement of end effectors to 90°, causes the helical microrobot to be steered in the opposite direction

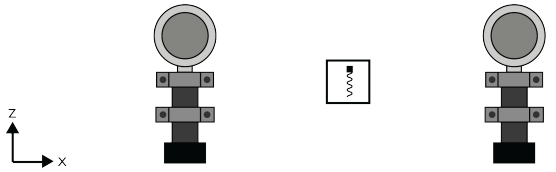

Fig. 2.8. Initial position of the system

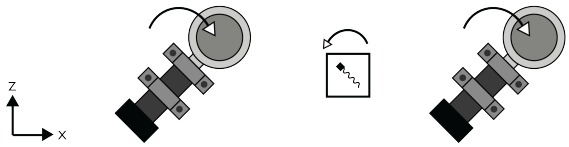

Fig. 2.9. Clock-wise movement of end effectors to 45°, causes the helical microrobot to be steered in the opposite direction

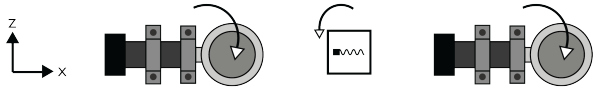

Fig. 2.10. Clock-wise movement of end effectors to 90°, causes the helical microrobot to be steered in the opposite direction

2.5.1 Magnetic field gradient forces compensation

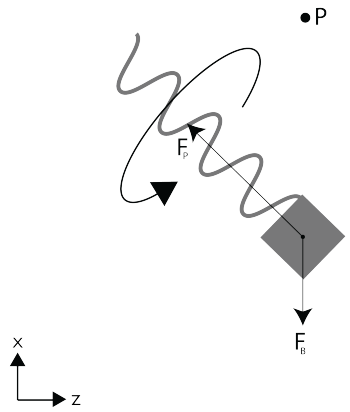

Fig. 2.11. The same strategy used for the gravity compensation can be used to mitigate the magnetic force caused by the field gradient, which appears as the microrobot is further away from the point P, the center of the workspace

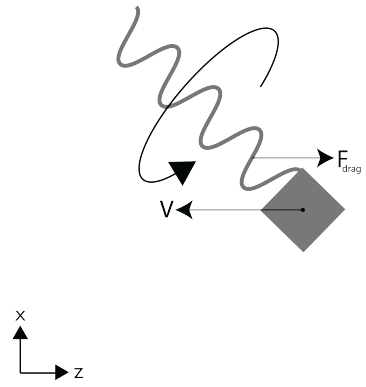

Fig. 2.12. The helical microrobot swims in the direction of the resultant force

2.6 Magnetic field in the axial direction caused by a cylindrical permanent magnet

$$B(x) = \frac{\mu_0 M}{2}\left(\frac{x}{\sqrt{x^2 + R^2}} - \frac{x - L}{\sqrt{(x - L)^2 + R^2}}\right)$$

$$\frac{\partial B(x)}{\partial x} = \frac{\mu_0 M}{2}\left(\frac{R^2}{(x^2 + R^2)^{1.5}} - \frac{R^2}{((x - L)^2 + R^2)^{1.5}}\right)$$

R is the radius of the permanent magnet, $B(x)$ is the magnetic field, x is the distance from the center of the magnet in the axial direction, L is the thickness of the magnet, μ_0 is the vacuum permeability constant and M is the dipole moment of the magnet. These equations are to be used in the design of the end effectors

3. FINITE ELEMENTS ANALYSIS

Finite elements analysis was done on the XZ plane of the mechanism to study the direction steering forces that act on the helical swimmer. Note that the results on the Z-axis can be also applied on the Y-axis, as the field changes the same way on both axes when axially magnetized cylindrical magnets are being used, so these results are applicable for both the direction and inclination steering forces. Results were achieved using Ansys 15.0 Mechanical APDL.

3.1 Preprocessor

Air and the Neodimium magnets were given a permability of 1. The magnets were axially magnetized with a coercive force of 900 kA/m. A customized mesh was generated to be high density with equally spaced nodes around point P, where the helical microswimmer should be, in order to get more accurate results.

3.2 Solution

For the solution of the analysis a magnetic vector potential formulation using maxwell equations was done.

3.3 Postprocessor

3.3.1 Magnetic field direction throughout the system

First analysis was done to show the direction of the resultant of the magnetic field at different points,

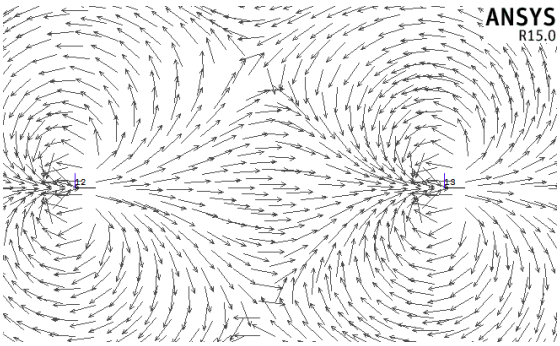

Fig. 3.1. Finite element analysis of the magnetic field induced by two cylindrical magnets in the XZ plane.

At this point of time it is observed in the analysis that the field in the center is oriented in the same direction of the magnetization of the magnets. However, the resultant of the field will then rotate in the opposite direction of the rotation of the end effector.

3.3.2 Magnetic field strength throughout the system

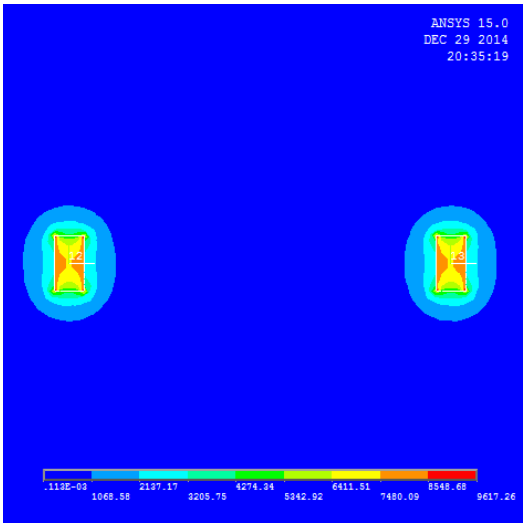

Fig. 3.2. Contour plot of the magnetic field strength induced by two cylindrical magnets

For the second analysis a counter plot of how the magnitude of the magnetic field varies with distance was created. However, the magnetic field changed so harshly around the end effectors compared to the rest of the field, that I was not able to show the changes at the midpoint.

The synchronous movement of the end effectors in both the radial and axial direction was studied, along with its effects on the magnetic field and its gradient.

The 5 cm point is the point when the helical microswimmer is in the midpoint between both end effectors (the point that was studied in the previous paper), and it can be observed that the gradient of the field tends to be zero in all axes.

However the area surrounding the midpoint would get a gradient and thus, an induced magnetic force on the microswimmer, this force can be observed to be inversely proportional the distance and thus, a resultant force perpendicular to the helical robot can be obtained by moving the end effectors the xyz plane.

3.3.3 Magnetic field strength and gradient in the workspace

It can be noticed at the 5cm point that the gradient is zero in both the axial and the radial graphs. This is due to the fact the both magnets cancel out the gradient forces at the center of the workspace.

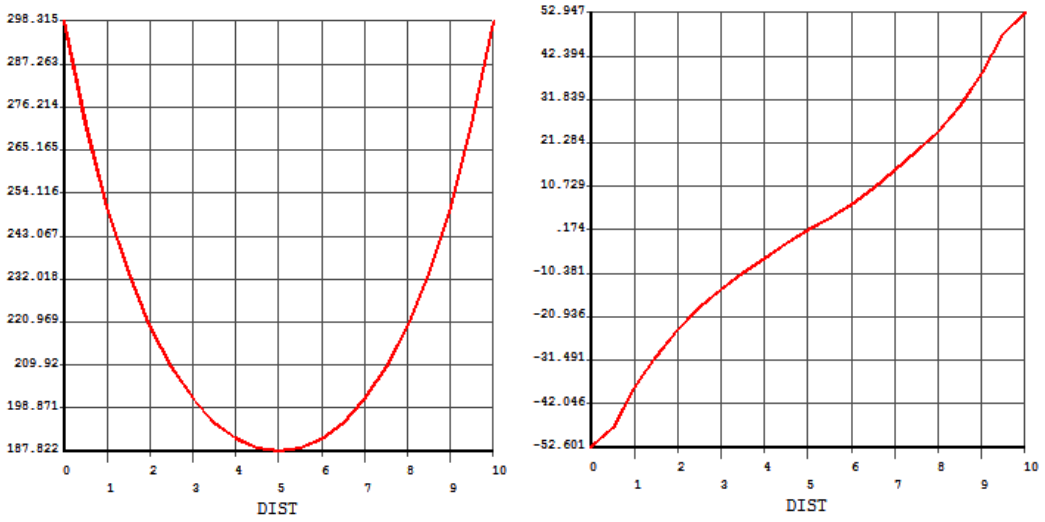

Fig. 3.3. Position of the end effectors in the axial direction in cm against the magnetic field in Gauss in the first graph, and against the gradient of the magnetic field in Gauss/cm

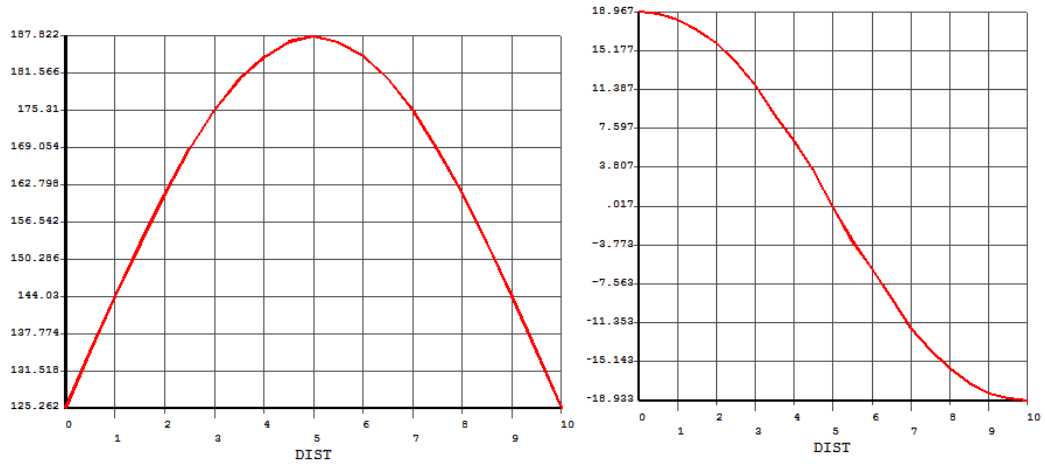

Fig. 3.4. Position of the end effectors in the radial direction in cm against the magnetic field in Gauss in the first graph, and against the gradient of the magnetic field in Gauss/cm

3.3.4 Single rotating dipole field

The analysis was redone using a single dipole field to analyse the results from the previous paper. It showed that the gradients in the radial direction are both zero; however, in the axial direction it is not zero, which means there will be a force towards the end effector.

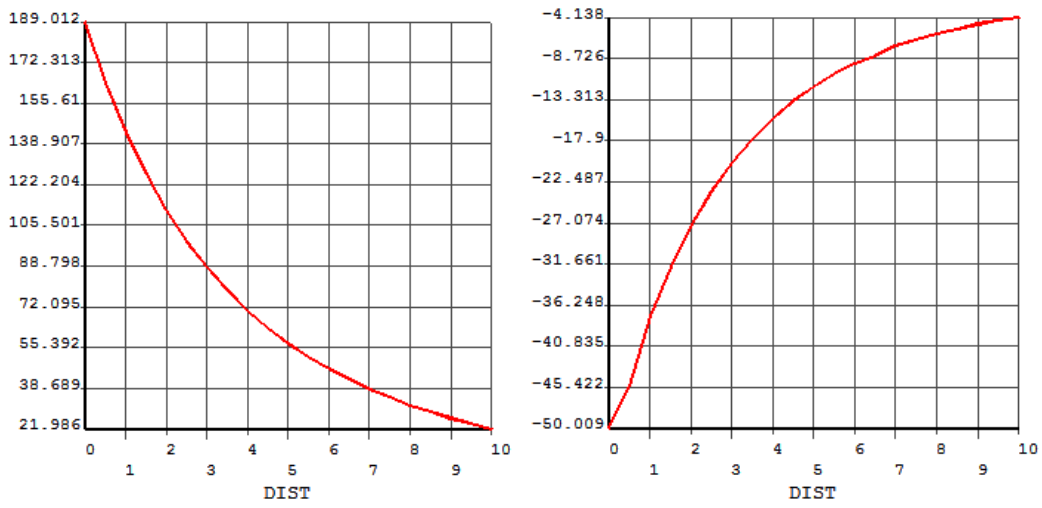

Fig. 3.5. Position of the end effectors in the axial direction in cm against the magnetic field in Gauss in the first graph, and against the gradient of the magnetic field in Gauss/cm

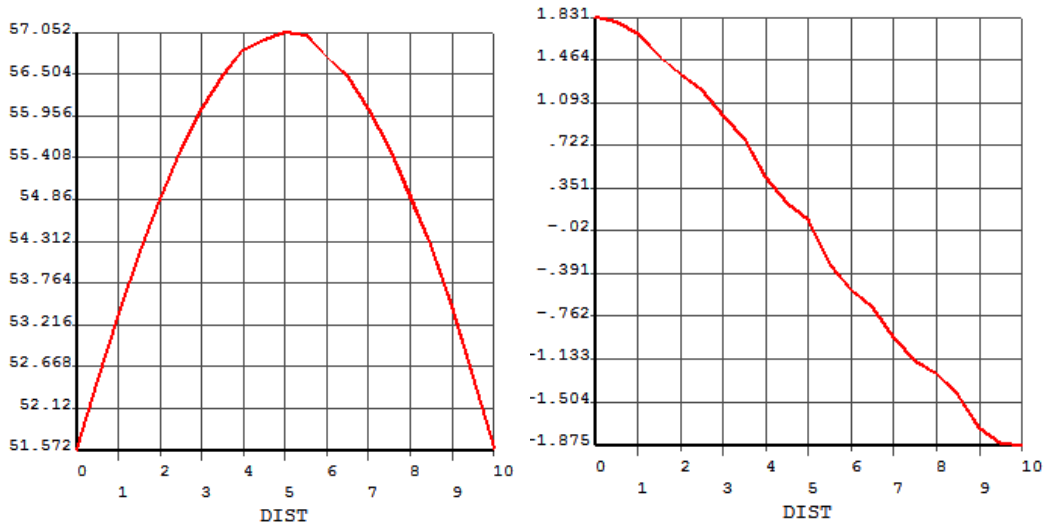

Fig. 3.6. Position of the end effectors in the radial direction in cm against the magnetic field in Gauss in the first graph, and against the gradient of the magnetic field in Gauss/cm

3.3.5 Fieldlines from steering the permanent magnets

The helical microrobot will automatically align itself to these field lines, and a magnetic torque will be applied on the helical microrobot whenever it is not aligned.

These results show the reason why the helical robot, when steered in the XZ plane, or on the u_t axis, rotates in the opposite direction of the end effectors.

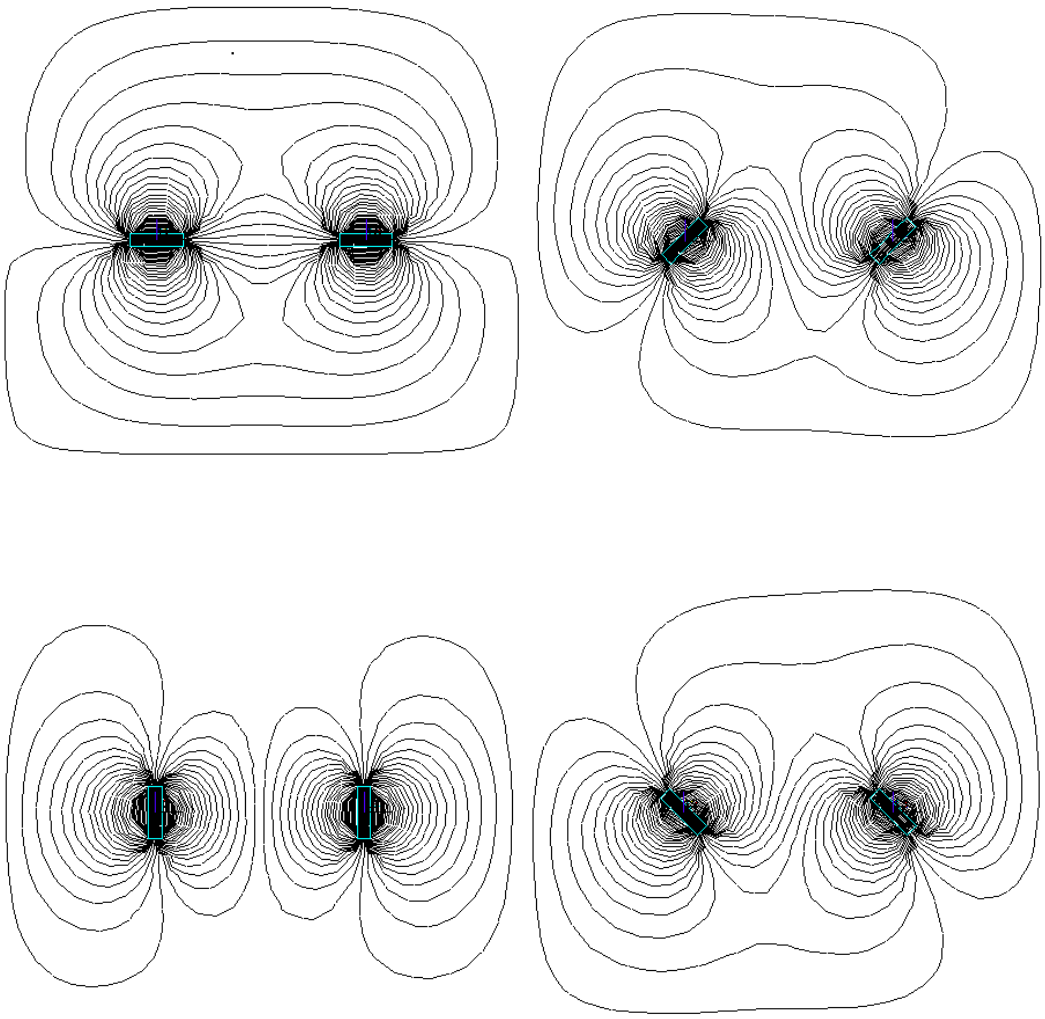

Fig. 3.7. Field lines plot analysis was made for long magnets to show how the field lines change with the steering of the permanent magnets

4. DESIGN AND DEVELOPMENT OF ROBOTIC SYSTEM

4.1 Mechanical Design

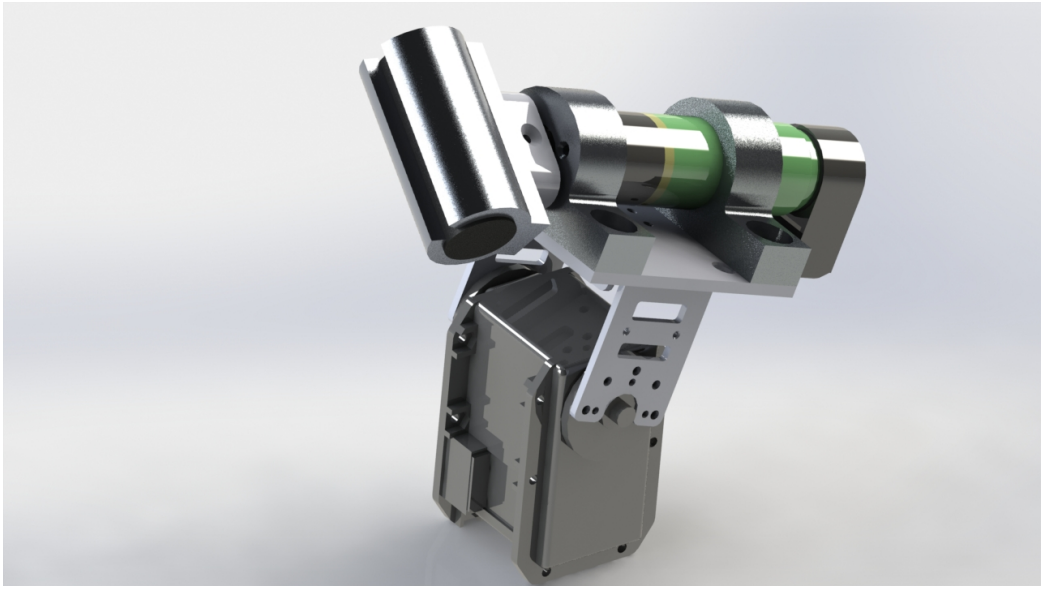

Fig. 4.1. A render of the design of the aluminum holders that fix the DC motor to the servomotor

All parts for the setup were designed on solidworks, and assembled together, it was designed with the limitation of CNC manufacturing in mind, all the screw sizes were also put into consideration so that the head of the screws would be sunk into the part.

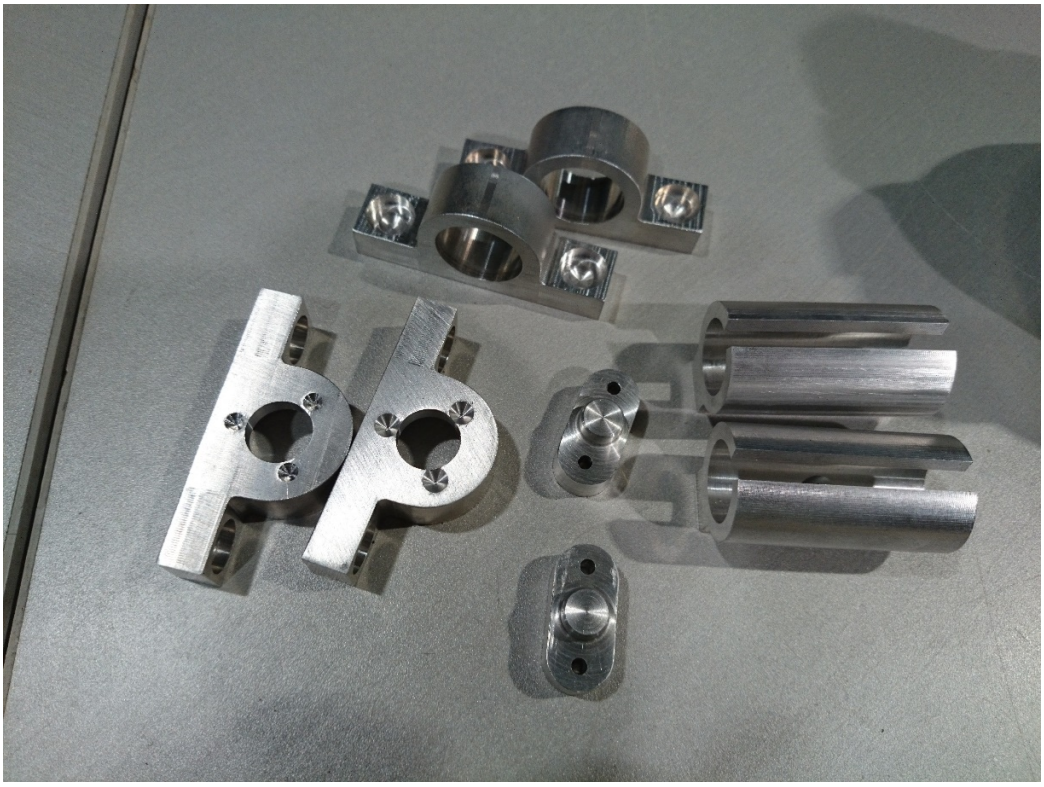

Fig. 4.2. The designs were manufactured in the GUC industrial park in a laser cutter machine, milling and drilling CNC machines

The parts designed on Solidworks were manufactured in the industrial park of the German University in Cairo, where all the parts were manufactured in CNC milling and drilling machines, some other parts were manufactured with laser cutting, all parts were produced with a percision of $1\mu m$, which helped making the system vibration free.

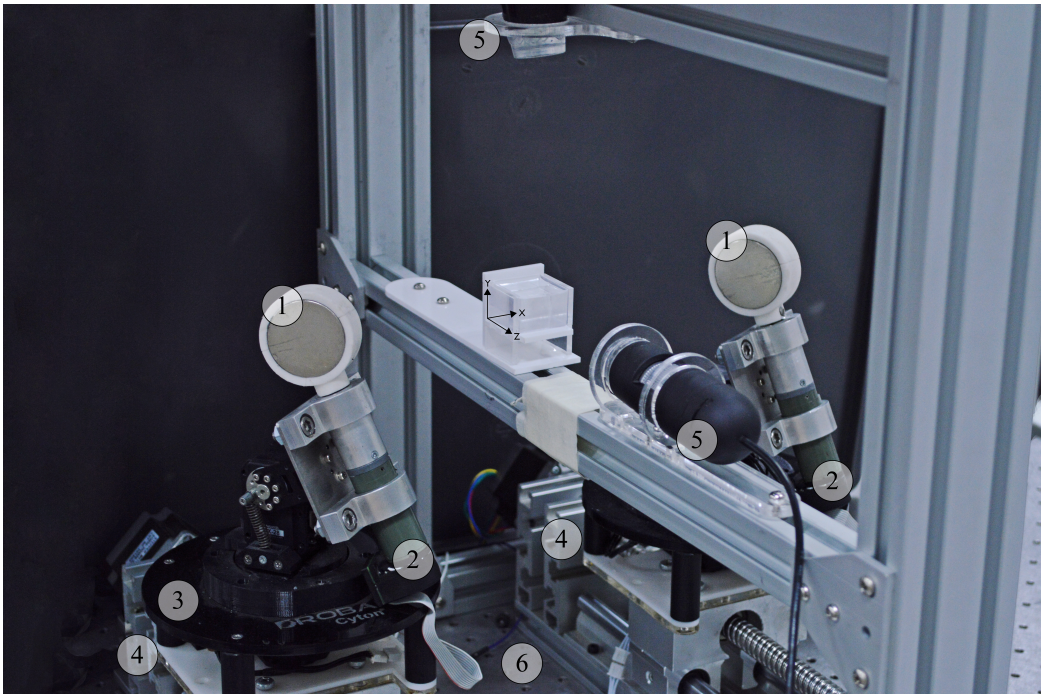

Fig. 4.3. The setup after all the parts were assembled together

Finally the robotic system was assembled out of two rotating permanent magnets ① using two DC motors ②. The motors are fixed on four servo motors ③ two servo motors on each side and travel along z-axis using two linear motion stages ④. The motion control three-dimensional space is done inside a water container . The motion of the helical microrobot is determined using two cameras ⑤. The system is mounted on a vibration isolation table ⑥.

4.2 Control

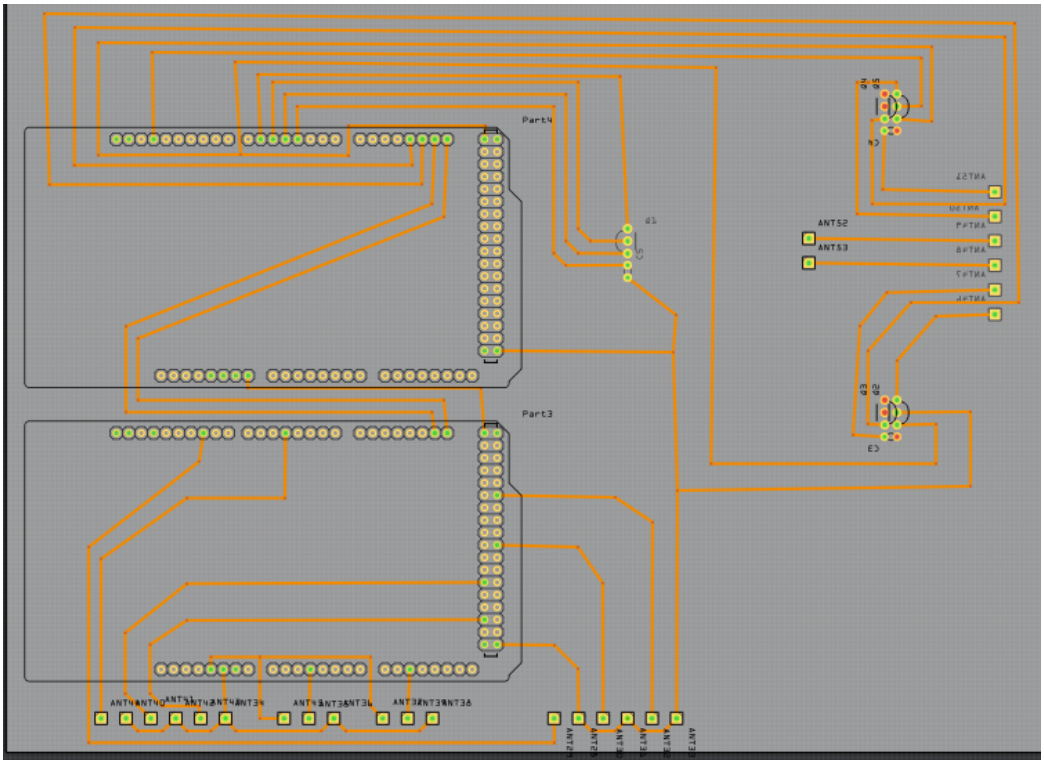

Fig. 4.4. Design of the PCB to connect 2 Arduino MEGA to a Dual channel DC motor driver and 2 stepper motor drivers

The control system consisted of a desktop computer taking visual input from 2 cameras and input from the user through the keyboard the camera on the side provides information for the XY plane, the one on top provides information for the XZ plane,a C++ code was written on the computer to processes these information, then communicates the changes to the microcontrollers 2 arduino boards (Arduino Mega 2560, Arduino, Memphis, Tennessee, USA)which controlled the closed-loop synchronization and the speed of the two DC motors (Maxon 47.022.022-00.19- 189 DC Motor, Maxon Motors, Sachseln, Switzerland)that rotates permanent magnets (N40 Neodymium, Amazing Magnets LLC, California, U.S.A) and they also do open-loop speed control on both stepper motors that run the linear stage, The C++ code

on the desktop computer also communicates with the USB2Dynamixel which controls 4 servo motors(Cyton Gamma 300, Robai, Cambridge, USA) in the robotic system, which indirectly control the orientation of the helical microbot

4.3 Down-scaling the helical microrobots

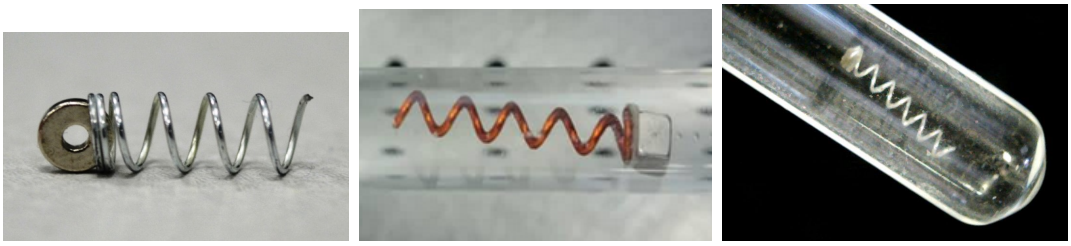

Fig. 4.5. on the left 4mm diamater helical microrobot, in the middle 2mm diameter, on the right 500μm diameter helical microrobot

we've worked on reducing the size of the helical microrobot, as the smaller we get the closer we get to medical applications, which makes the control more on point with the actual application since we are operating on a lower reynold's number, until the smallest we could manufacture was the size of 500μm diameter(Neodymium N42 magnetic head, Aluminum helical tail) The microrobots used in all the experiments in this thesis followed the same design of this microrobot.

5. EXPERIMENTAL RESULTS

5.1 Tesla experiments

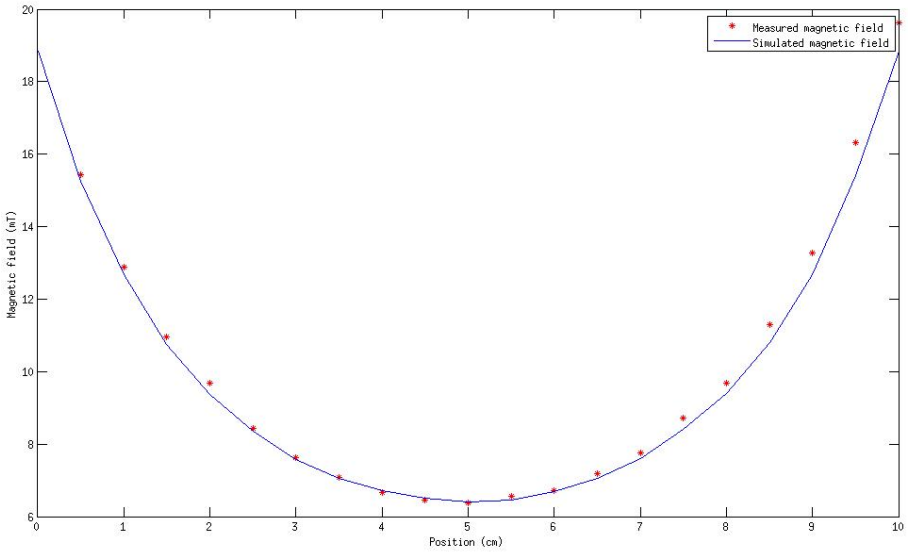

Fig. 5.1. Position of the helical robot in the axial direction in cm against the the magnetic field

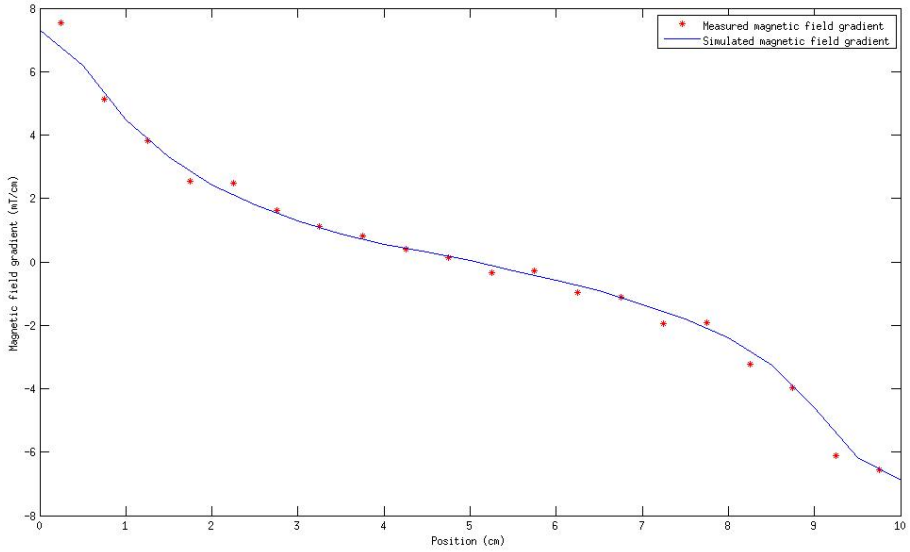

Fig. 5.2. Position of the helical robot in the axial direction in cm against the gradient of the magnetic field

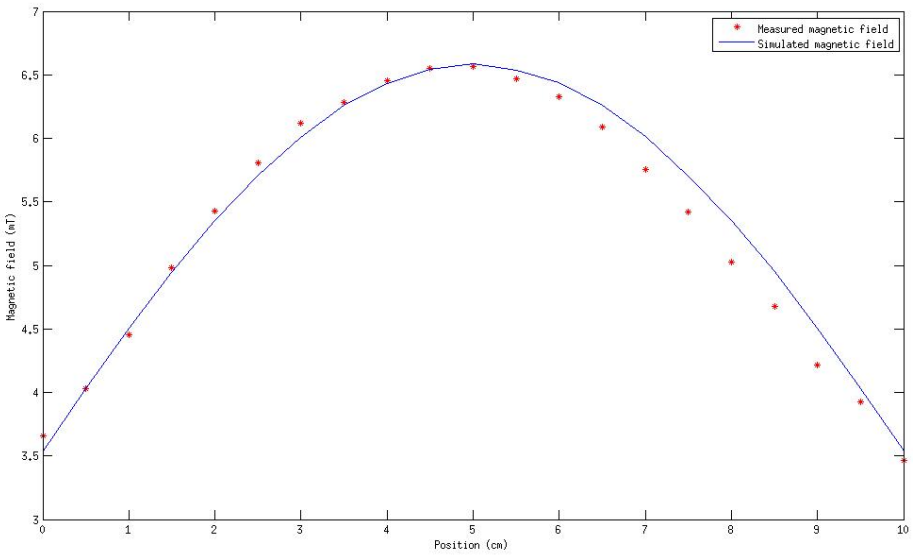

Fig. 5.3. Position of the helical robot in the radial direction in cm against the the magnetic field

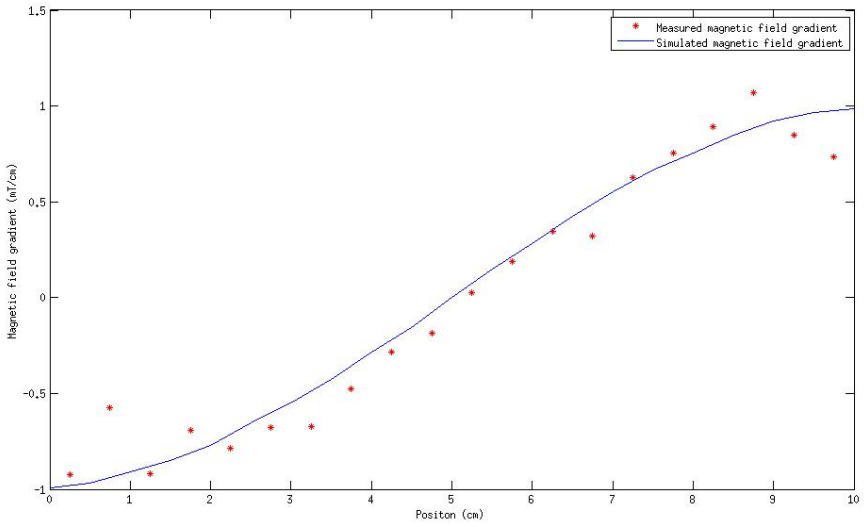

Fig. 5.4. Position of the helical robot in the radial direction in cm against the gradient of the magnetic field

The magnetic field in the workspace was measured using a teslameter (Sensis 3MH3 Teslameter) with a 3-axis Hall Probe, measurements were taken with the end effectors (N40 Neodymium, Amazing Magnets LLC, California, U.S.A) at a 90° measurements were taken in a $10cm \times 10cm$ workspace at a $1cm$ increment each. The measurements taken on the X-axis and the Z-axis were plotted on a graph.

Due to the permanent magnet being a cylinrical magnet the measurements taken on the Z-axis, was similar to the readings taken in the Y-axis, the reason it wasnt the same readings, was due to the ferrite material affectting the magnetic field in the workspace, like for example the optical table, however the reading should be the same on any axis in the radial direction of the permanent magnet.

5.2 Propulsion control

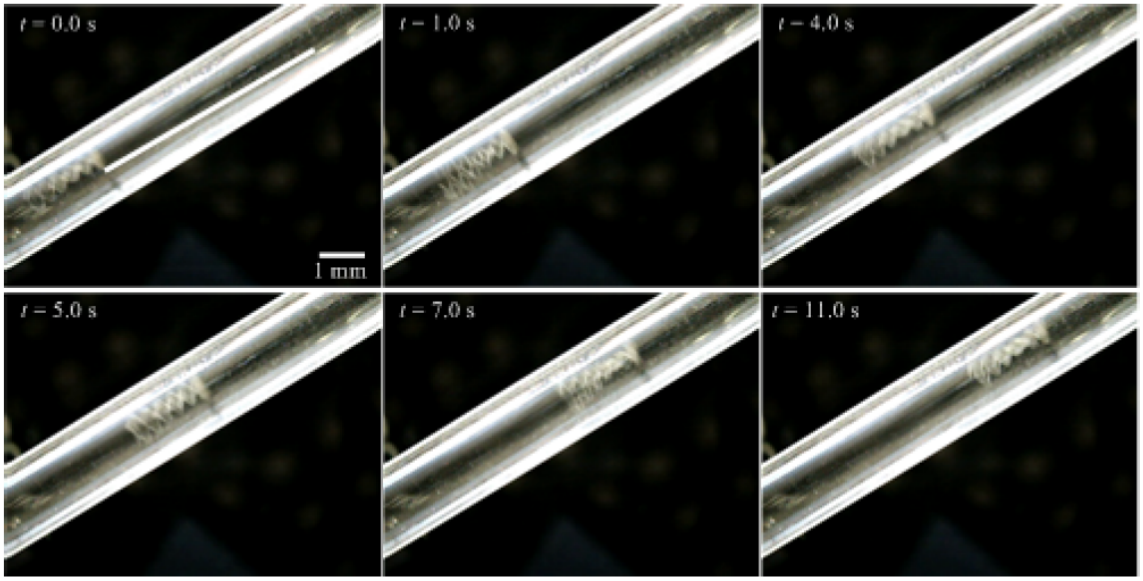

Fig. 5.5. One-dimensional control of a helical microrobot with a diameter of 500 μm inside a tube, under the influned of two synchronized rotating dipole fields of 8 Hz it swam at an average speed of $483\mu m/s$

A scaled up propulsion control experiment was conducted before [6] so it was conducted again in microscale after we were first able to manufacture our first robot in micro-scale, 500 μm diameter. the main purpose of the experiment was to test the propulsion of the robot, and the ability of the system to mitigate the gradient forces and minimizing the lateral oscillations, however we noticed some lateral oscillation during the propulsion of the helical microrobot, but we later found out the reason for this oscillations was due to a problem in the closed loop synchronization of the DC motors(which was then fixed), and the dipole moment wasnt exactly perpendicular to the direction of the helical structure (different microrobots were later manufactured with better alignment of parts) the lateral oscilations needed to be completely mitigated to allow the system to control the microrobot in three-dimensional space.

5.3 Two-dimensional steering

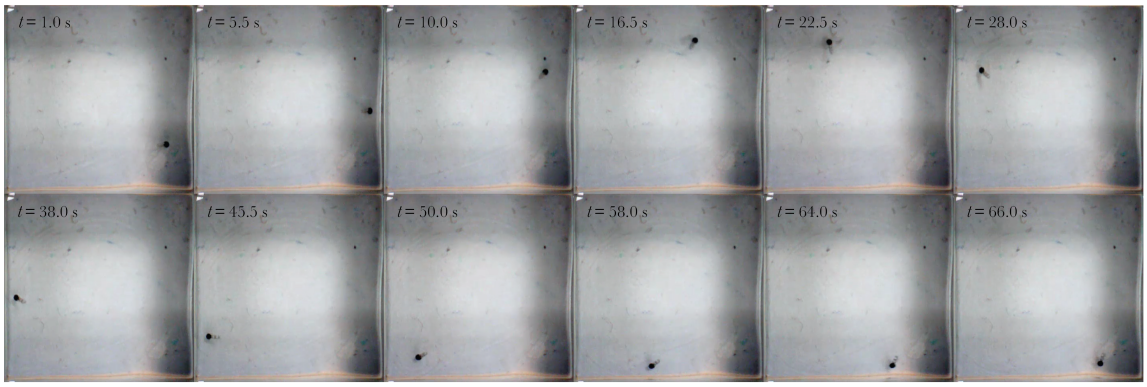

Fig. 5.6. An experiment for motion control of a helical microrobot with a diameter of 500 μm inside a water reservoir in two dimensional (2D) space, the helical robot is to follow a circular trajectory in open-loop.

The experiment was done to prove that the two-synchronized dipole fields system is capable of doing two dimensional control on the helical microrobot, however the experiment ultimately failed due to a factor that wasnt predicted before the experiment, which was that since the helical microrobot was doing it's locomotion on the bottom floor of the container, the helical microrobot was transporting itself by rolling on the ground, not propelling itself through the liquid, eventhough the experiment did fail, it still proved that we are capable of steering the helical microrobot with this system.

5.4 Two-dimensional control

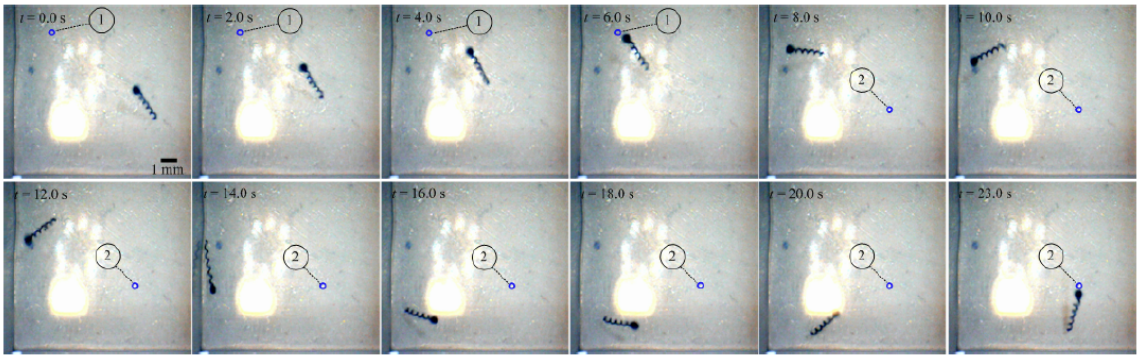

Fig. 5.7. A representative motion control result of a helical microrobot with a diameter of 500 μm inside a water reservoir in two dimensional (2D) space. The microrobot swims at an average speed of 875 m/s under the influence of two synchronized rotating dipole fields. The frequency of the rotating dipole fields is 8 Hz. The angle between the axis of the helical microrobot and z-axis is 20 . This angle does not generate enough propulsive force component to compensate for the force due to gravity. The small blue circles indicate two reference positions. The rotating dipole fields allow the microrobot to orient towards the reference position and achieve helical propulsion towards them. oscillations.

In these experiments we attempted to lift the helical microrobot's head and by steering the helical microrobot in the ZY plane, in one of the experiments the microrobot was capable of being controlled in two-dimensional space, and to go to reference position, however since the robot's magnetic head had a high density, it's center of mass was closer to the head, so any slight disturbances caused the microrobot's head to drop to the ground of the container. which then causes the microrobot to roll instead of propel itself.

5.4.1 System upgrades

The system was not robust enough to keep the helical microrobot repeat the same experiment, and it wasnt capable of doing three-dimensional control on the helical microrobot, so a number of changes were made to the system.

1. The number of turns in the helical microrobot's tail was increased from 6 turns to 4; increasing the propulsive force of the microrobot but at the cost of requiring a higher magnetic torque.

2. Due to the helical microrobot required a higher magnetic field to operate in it's enviroment, we bought two powerful neodymium permanent magnets (N40 Neodymium, Amazing Magnets LLC, California, U.S.A) and a couple of holders were manufactured using 3D printing to attach it to the setup

3. The distance between both of the end effectors were increased to 40 cm, to decrease the effect of the magnetic field gradient on the helical microrobot when it isnt in the center of the workspace

4. The helical microrobot is controlled using backwards propulsion to reduce the effect of the torque caused from the weight of the magnetic head

5.5 Gravity compensation

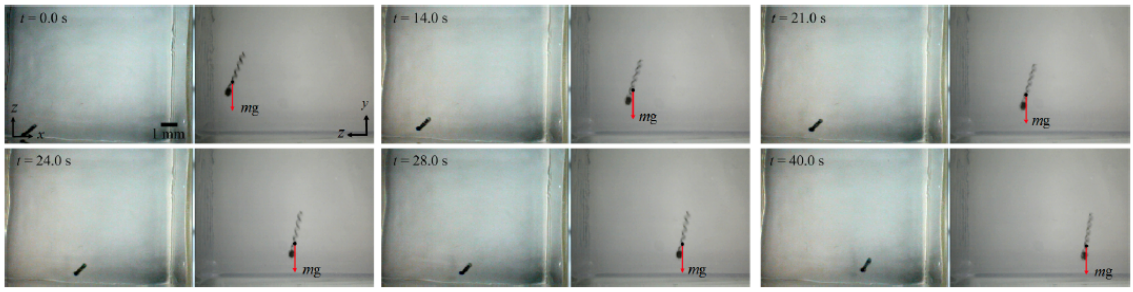

Fig. 5.8. Motion control of a helical microrobot in three-dimensional space under the influence of two synchronized rotating dipole fields. The microrobot swims and compensates gradient forces and the force due to gravity (mg), m is the mass of the microrobot and g is the acceleration due to gravity. The helical microrobot swims at an average speed of 196.1 $\mu m/s$ and rotates at frequency of 8 Hz. We observe that the helical microrobot compensates for gravity and moves upward at,$\phi = 63°$ oscillations.

After the system was upgraded, The helical microrobot was capable of lifting itself off the ground and then suspending itself in the container, it was able to compensate for gravity with the Y-axis component of it's propulsion force, which gave us the ability to control the helical microrobot in two-dimensional space (2D) and three-dimensional space (3D)

5.6 Three-dimensional control

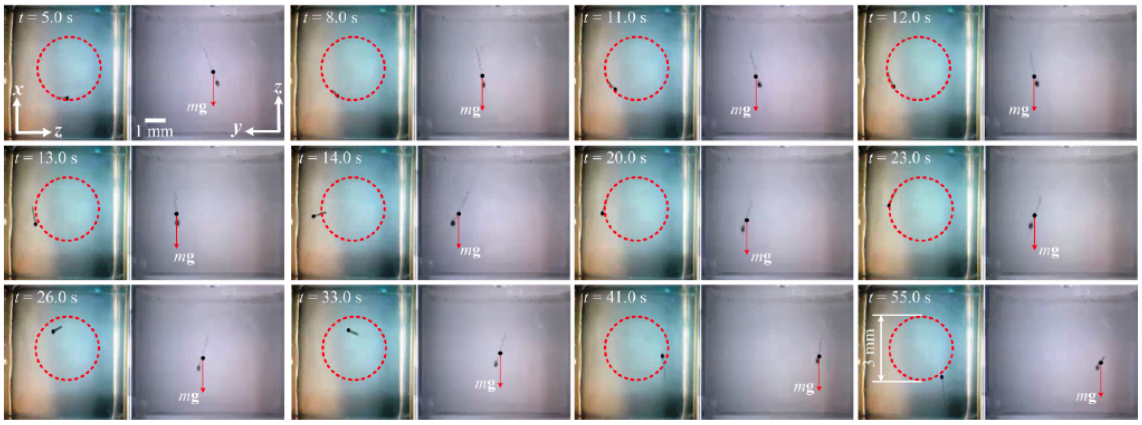

Fig. 5.9. A representative motion control result of the helical microrobot in three-dimensional (3D) space. The helical microrobot is following a circular trajectory in xz-plane with a diameter of 3 mm. The force (mg) due to gravity is compensated by the helical propulsion of the microrobot (yz-plane), where m is the mass of the microrobot and g is the acceleration due to gravity. The average speed of the helical microrobot is calculated to be 171 $\mu m/s$, at frequency of 8 Hz of the rotating dipole fields. oscillations.

The image on the left side of each frame is the top view (XZ plane) while the image on the right is the side view (XY plane), The helical microrobot was able to follow a circular trajectory, while at the same time compensating for the gravity and the gradient forces, the microrobot was oriented so that the resultant of all the forces directs the robot to follow the circular pattern.

6. SUMMARY

We designed and built a new setup to control helical microrobots in an open loop configuration, using two synchronized rotating dipole fields, our finite element analysis proved that the system cancels out the gradient of the magnetic field, and reduces it's effect throughout the workspace, our experimental results proved that our system was able to control the helical microrobot in three-dimensional space with gravity and gradiant forces compensation, and what remains of the gradient forces is compensated using propulsion force, the helical microrobot also compensated for gravity using the y-axis component of the propulsion force, and we observe that the helical microrobot, The steering strategy used in the system, when the helical robot is steered in the XZ plane, it robotates in the opposite direction of the rotation of the end effector, while the rotation in the YZ plane and the XY plane is the same as the rotation of the end effectors.

7. RECOMMENDATIONS

After building the setup and doing experiments, there are some recommendations, if the setup is to be rebuilt, to provide more robust results, better suited for vivo applications.

- Optimize the shape of the permanent magnets, a longer and thinner magnet will provide a bigger field and lower gradient, allowing us to build a bigger setup, and a more robust control
- Study the effect of using more than one end effector in the control, this could be used for the control of a swarm of helical microrobots
- The setup does provide a self stabilizing feature when the microrobot is moved in the ZY plane, this could be study for control against flow
- Study the ability of the robotic system to control microrobots other than the helical microrobot
- In our robotic system we use 4 servo motors to indirectly control the steering of the helical microrobot however the length of the links in this system, causes a change in the gradient of the magnetic field when the microrobot is steered, comming up with a new design to be able to steering the rotating permanent magnet without moving it in three dimensional space, will lead to a more robust control
- Implement a closed-loop algorithms using input from the cameras to make the microrobot automatically compensate for the gravity and gradient forces

LIST OF REFERENCES

LIST OF REFERENCES

[1] E. M. Purcell, "Life at low reynolds number," *American J. Physics*, vol. 45, pp. 3–11, 1977.

[2] I. S. M. Khalil, H. C. Dijkslag, L. Abelmann, and S. Misra, "Magnetosperm: A microrobot that navigates using weak magnetic fields," *Applied physics letters*, vol. 104, 2010.

[3] I. S. M. Khalil, P. Ferreira, R. Eleuterio, C. L. de Korte, and S. Misra, "Magnetic-Based closed-loop control of paramagnetic microparticles using ultrasound feedback," in *Proceedings of the IEEE International Conference on Robotics and Automation (ICRA)*, pp. 3807–3812, June 2014.

[4] D. de Lanauze, O. Felfoul, J.-P. Turcot, M. Mohammadi, and S. Martel, "Three-dimensional remote aggregation and steering of magnetotactic bacteria microrobots for drug delivery applications," *The International Journal of Robotics Research*, vol. 28, pp. 359–374, 2014.

[5] K. E. Peyer, L. Zhang, and B. J. Nelson, "Bio-inspired magnetic swimming microrobots for biomedical applications," *Nanoscale*, vol. 5, pp. 1259–1272, 2012.

[6] M. E. Alshafeei, A. Hosney, A. Klingner, S. Misra, and I. S. M. Khalil, *Magnetic-Based motion control of a helical robot using two synchro- nized rotating dipole fields, in Proceedings of the IEEE RAS/EMBS International Conference on Biomedical Robotics and Biomechatron- ics (BioRob).* Aug. 2014.

[7] a. G. H. Tiantian Xu, N. Andreff, and S. R. , "Characterization of three-dimensional steering for helical swimmers," *2014 IEEE International Conference on Robotics and Automation (ICRA)*, pp. 4686 – 4691, 2014.

[8] A. W. Mahoney, J. C. Sarrazin, E. Bamberg, and J. J. Abbott, "velocity control with gravity compensation for magnetic helical microswimmers, Advanced Robotics," vol. 28, pp. 1007–1028, Apr. 2012.

[9] M. P. Kummer, J. J. Abbott, B. E. Kartochvil, R. Borer, A. Sengul, and B. J. Nelson, "Octomag: an electromagnetic system for 5-dof wireless micromanipulation," *IEEE Transactions on Robotics*, vol. 26, pp. 1006–1017, 2010.

[10] A. W. Mahoney, D. L. Cowan, K. M. Miller, and J. J. Abbott, *Control of untethered magnetically actuated tools using a rotating permanent magnet in any position, in Proceedings of the IEEE International Conference on Robotics and Automation (ICRA).* May 2012.

[11] T. W. R. Fountain, P. V. Kailat, and J. J. Abbott, *Wireless control of magnetic helical microrobots using a rotating-permanent-magnet manipulator, in Proceedings of the IEEE International Conference on Robotics and Automation (ICRA).* may 2010.